Supporting Online Material for

Dynamical Response of the Tropical Pacific Ocean to Solar Forcing During the Early Holocene

Thomas M. Marchitto,* Raimund Muscheler, Joseph D. Ortiz, Jose D. Carriquiry, Alexander van Geen

*To whom correspondence should be addressed. E-mail: tom.marchitto@colorado.edu

Published 3 December 2010, *Science* **330**, 1378 (2010)
DOI: 10.1126/science.1194887

This PDF file includes:

Supporting Online Material

Modern hydrographic data

Local SSTs are from NOAA's National Centers for Environmental Prediction (NCEP) weekly 1° grid optimum interpolation analysis (version 2) using in situ and satellite SSTs (*1*). The Niño3 index is calculated from the same SST database. Both data sets are available at http://iridl.ldeo.columbia.edu/SOURCES. We note that the Soledad Basin correlation to ENSO (r = 0.61) is considerably stronger than to the related Pacific Decadal Oscillation (PDO) index (r = 0.36) (*2*). The upwelling index (offshore Ekman transport) is calculated by NOAA's Pacific Fisheries Environmental Laboratory (PFEL) using atmospheric pressure fields prepared by the U.S. Navy Fleet Numerical Meteorological and Oceanographic Center (FNMOC) (*3*). Data are available at the PFEL website (http://www.pfeg.noaa.gov/).

Age model

Twenty three foraminiferal samples were radiocarbon dated by accelerator mass spectrometry (AMS): 11 from GC41 (10 planktonic and 1 benthic) and 12 from PC14 (10 planktonic and 2 benthic) (Table S1). Three of the GC41 dates and all of the PC14 dates were previously published *(4)*. The published dates were on mixed planktonics (mostly the surface dwelling species *G. bulloides* and *G. ruber*) and mixed benthics (mostly *Bolivina* spp.), while the new dates were on monospecific *G. bulloides*. All dates were recalibrated using the online program Calib 6.0html (*5*) and the Marine09 calibration curve (*6*). We used reservoir age corrections (ΔR) of 200 ±100 yr for the planktonic ages (*4*) and 400 ±100 yr for the benthic ages. Age models were fit through the median calibrated ages from each core, using a straight line in GC41 and a 4^{th}-order polynomial in PC14 (Fig. S1A). Based on our previous work documenting the incursion of radiocarbon-depleted waters during Heinrich Stadial 1 and the Younger Dryas (*7*), we omit one date that falls within the interval that corresponds to the Younger Dryas according to our diffuse spectral reflectance (DSR) stratigraphy (Fig. S1B). After then placing the core on the resulting radiocarbon age model, the DSR change that signals the end of the Younger Dryas matches the Greenland ice core (GISP2) age of this event (*8*) within 50 yr (Fig S1).

Mg/Ca methods

Samples consisting of typically ~30-60 specimens of *G. bulloides* (250-355 μm) were crushed between glass microscope slides, with larger samples being split into two aliquots for replicate measurements. Crushed samples were cleaned reductively (using anhydrous hydrazine) and oxidatively (using H_2O_2) in a Class-1000 clean lab (*9, 10*). Multiple minor and trace elements were measured by magnetic-sector single-collector ICP-MS, on a Thermo-Finnigan Element2 (*11, 12*). Long-term 1σ precision for Mg/Ca, based on analysis of consistency standard solutions, is 0.5% across a wide range of Mg/Ca values and sample sizes.

Of 442 Mg/Ca measurements that met the minimum size cutoff of >5 μg $CaCO_3$, 5 were discarded because they yielded a standard deviation with their replicates that was >0.5 mmol mol^{-1}. The pooled standard deviation of the remaining replicates was 0.18 mmol mol^{-1} (dof = 213). Many of these replicates were based on separate samplings of the same interval, which leads to greater scatter than split aliquots of a crushed sample. An additional 4 unreplicated measurements were discarded because their standard deviation with one or both of their neighboring means was >0.7 mmol mol^{-1}. The total rejection rate was therefore 2.0% (9/442). Amongst all 442 samples, Mn/Ca was never >15 μmol mol^{-1}, indicating negligible carbonate

overgrowths. Fe/Ca was >200 μmol mol^{-1} in 6 samples and Al/Ca was >200 μmol mol^{-1} in 5 samples, but their Mg/Ca data were not excluded because they were not outliers. The >500-yr data gaps near 2 and 6 ka are due to relatively low abundances of *G. bulloides*.

Mg/Ca was converted to SST using a calibration based on laboratory-grown *G. bulloides* combined with core top samples (*13*), which has been verified using sediment trap samples from Santa Barbara Basin off of southern California (*14*). The standard error of this equation is quoted at ±0.8°C (*13*).

Cross wavelet analysis

To identify common spectral power and its phase relationship between the unsmoothed Mg/Ca data and the cosmogenic nuclide proxies, we computed cross wavelet transforms (*15*) (Fig. S2). Only the very high resolution portion of the Mg/Ca record was used (>6.5 ka, prior to the data gap). Data were first interpolated to 50 yr spacing (based on the nominal spacing of the Mg/Ca series) and linearly detrended. Strongest common power is at periods of ~800-1000 yr, significant at the 95% confidence level. Significant common power extends forward to ~8.5 ka versus ^{14}C production and to ~9.5 ka versus ^{10}Be flux. Phase angle within these regions ranges from 0° to a slight lag on Mg/Ca. At ~8-8.5 ka the common power diminishes and the lag grows, especially for ^{10}Be (~90°), probably because of the '8.2 ka event' as noted in the main text. The phase relationship with ^{10}Be is different from that with ^{14}C because the age models of the two cosmogenic time series differ (see Fig. 3). The tree-ring based chronology for ^{14}C (*16*) is believed to be more precise and accurate than the ice core chronology for ^{10}Be (*17*).

Data processing for comparing multi-centennial/millennial signals

Data processing to further examine the proposed relationship between solar forcing and the various proxy time series was motivated by two necessities. First, we wished to smooth the Mg/Ca series to eliminate high-frequency variability. This variability likely represents a combination of real climate fluctuations that are at too high a frequency to reliably correlate to other records (due to aliasing and age uncertainties), plus some proxy-related noise. We chose a 5-depth running mean, which equates to roughly 200-300 yr. We decided to smooth rather than lowpass filter so that the smoothed record would be based on actual measurements (since filtering requires interpolation first). The other records were smoothed at ~250 yr to match the Mg/Ca treatment as closely as possible. Second, we wished to remove long-term drift from the nuclide records that is likely related to slow variations in the geomagnetic field (*18*). We detrended and FFT highpass filtered each record at 1/1800 yr, following Bond et al. (*19, 20*). Although the best frequency cutoff is not known, the results are not very sensitive to this choice (Fig. S3). The proxy records were filtered in the same way to remove drift that is unlikely to be driven by solar variability. We aimed to be as consistent as possible in processing each record, but differences in sample spacing necessitated slightly different approaches.

Soledad Basin Mg/Ca: We calculated the running mean of individual values from 5 consecutive depths in the core (Fig. 3A), followed by 50-yr interpolation, linear detrend, and 1/1800 yr highpass filter (Fig. 4).

^{14}C production rate: Production rate after the end of the Younger Dryas was first calculated from IntCal04 $\Delta^{14}C$ data (*16*) using a box-diffusion model with the carbon cycle held constant (*21-23*). We then calculated the 251-yr running mean of annual production rate data, followed by linear detrend, 1/1800 yr highpass filter, and 50-yr resampling (Fig. 3B, 4).

^{10}Be flux: Flux after the end of the Younger Dryas was first calculated from GISP2 (*24*) and GRIP (*25*) ^{10}Be records, which combined provide a continuous Holocene record. Records were combined after correcting for differences between average ^{10}Be concentrations for periods of overlap and after correcting for timescale differences between the GRIP and GISP2 chronologies. Flux data is reported on the GICC05 timescale (*17*), which was also used to derive accumulation rates for the flux calculations. Thinning of layers due to ice flow was corrected for using the strain rate from the ss09sea model (*26*). We then calculated the 249-yr running mean of interpolated biennial flux data, followed by linear detrend, 1/1800 yr highpass filter, and 50-yr resampling (Fig. 3C, 4).
Dongge Cave $\delta^{18}O$: Using data on untuned U-Th age model (*27*). We performed a 5-yr interpolation, followed by 250-yr running mean, linear detrend, 1/1800 yr highpass filter, and 50-yr resampling (Fig. 4).
Hoti Cave $\delta^{18}O$: Using data on untuned U-Th age model (*28*). We performed a 5-yr interpolation, followed by 250-yr running mean, linear detrend, 1/1800 yr highpass filter, and 50-yr resampling (Fig. 4).
Bond IRD stack: Using 70-yr interpolated stack data on untuned calibrated ^{14}C age model (*19*). We calculated the 3-point running mean, followed by 50-yr interpolation, linear detrend, and 1/1800 yr highpass filter (Fig. 4).

Fig. 3 shows that for the nuclide records, both the approach described above (black) and the 1/1800-1/500 yr bandpass approach of Bond et al. (*19, 20*) (pink) capture the multi-centennial to millennial scale variability inherent in the original data.

The running 2σ error envelope on Mg/Ca shown in Fig. 3A is based on the standard error of mean values from 5 consecutive depths, where n is the total number of individual measurements in that interval. Correlation coefficients were calculated at various time lags. We report the maximum correlation found within several 50-yr time steps. The greatest lag found was 100 yr, which is well within the combined age uncertainty of the various time series comparisons. Therefore we do not consider the lag magnitudes themselves to be meaningful. P-values were calculated using the reduced degrees of freedom that resulted from smoothing the Mg/Ca record (dof = (n-2)/5, where n is the number of time steps that the correlation is calculated over).

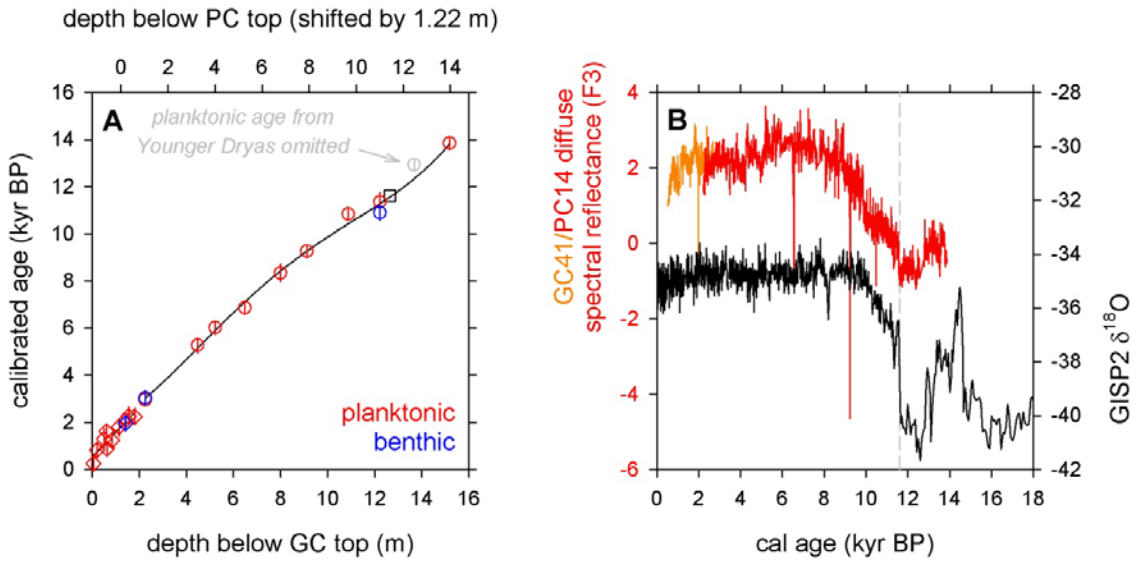

Fig. S1. (**A**) Polynomial age models (black lines) fit through calibrated radiocarbon ages from GC41 (diamonds) and PC14 (circles). Symbols are median ages with 2σ error ranges. Gray date was omitted from the fit (see text). Black square denotes the age of the end of the Younger Dryas in Greenland ice core GISP2 (*8*) and the depth of this event in PC14 as inferred from the DSR record shown in panel (**B**). This point was not used in generating the polynomial age model. The depth scales for the two cores are offset according to (*4*) but this detail has no effect on the age models. (**B**) GC41/PC14 DSR factor 3, which exhibits a strong correlation to productivity proxies along this margin (*7, 29*), plotted on the age models from panel (**A**) and compared to GISP2 $\delta^{18}O$ (*8*). Previous work has shown that DSR stratigraphies from this region closely mimic Greenland $\delta^{18}O$, with abrupt transitions likely being synchronous (*7, 29*). Gray dashed line denotes the GISP2 age of the end of the Younger Dryas (11.61 ka).

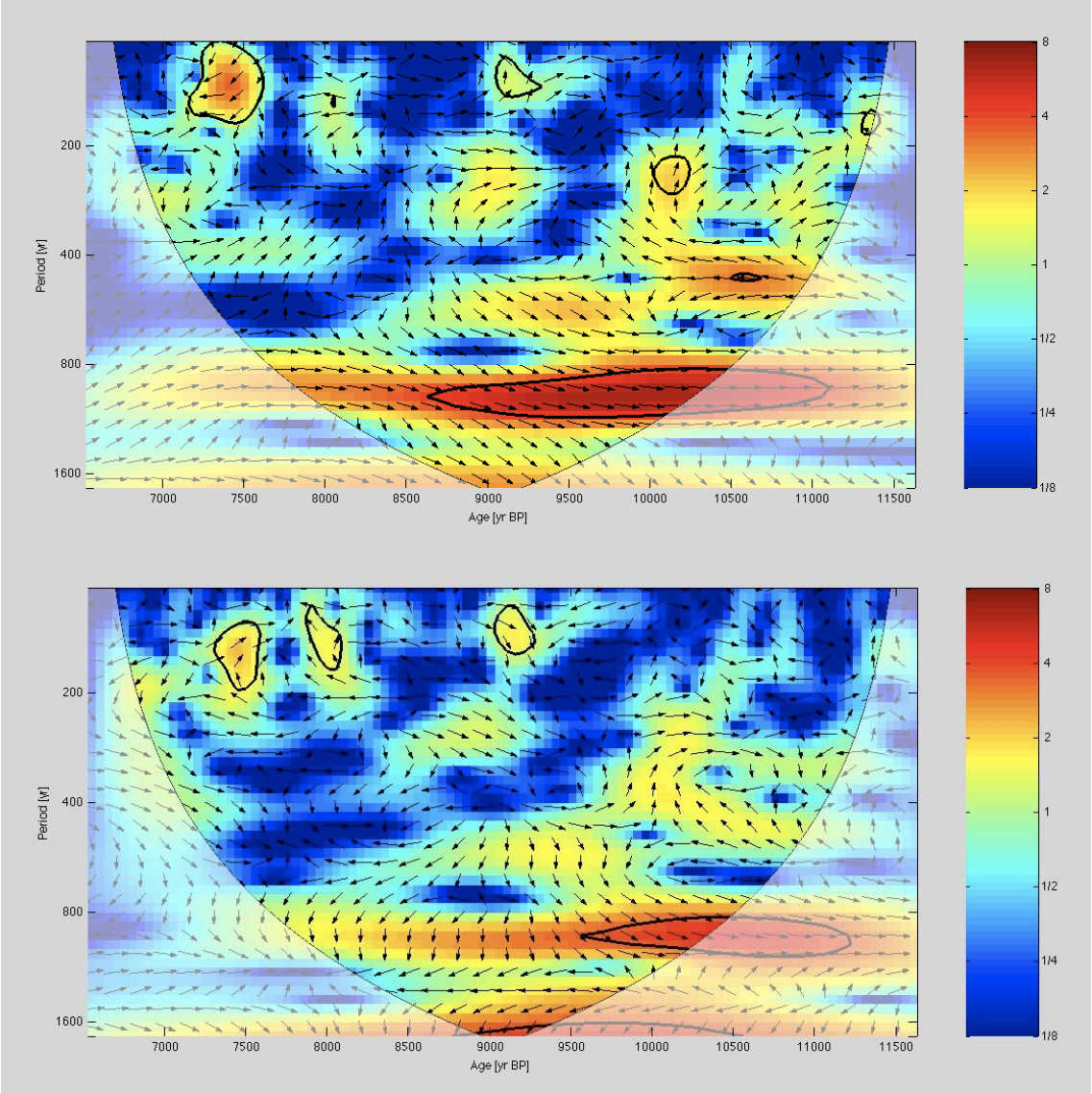

Fig. S2. Cross wavelet transforms (*15*) of Soledad Basin Mg/Ca vs. (top) cosmogenic ^{14}C production and (bottom) ^{10}Be flux. Warm colors indicate regions of high common spectral power between the two time series. Regions within bold black contours are significant at the 95% confidence level against red noise. Small areas of significant common power at short periods (~100-300 yr) are not meaningful because of age model uncertainties. Arrows denote phase angle, with in-phase pointing right, anti-phase pointing left, and 90° lag on Mg/Ca pointing down. Clouded region denotes the Cone of Influence where edge effects cannot be ignored.

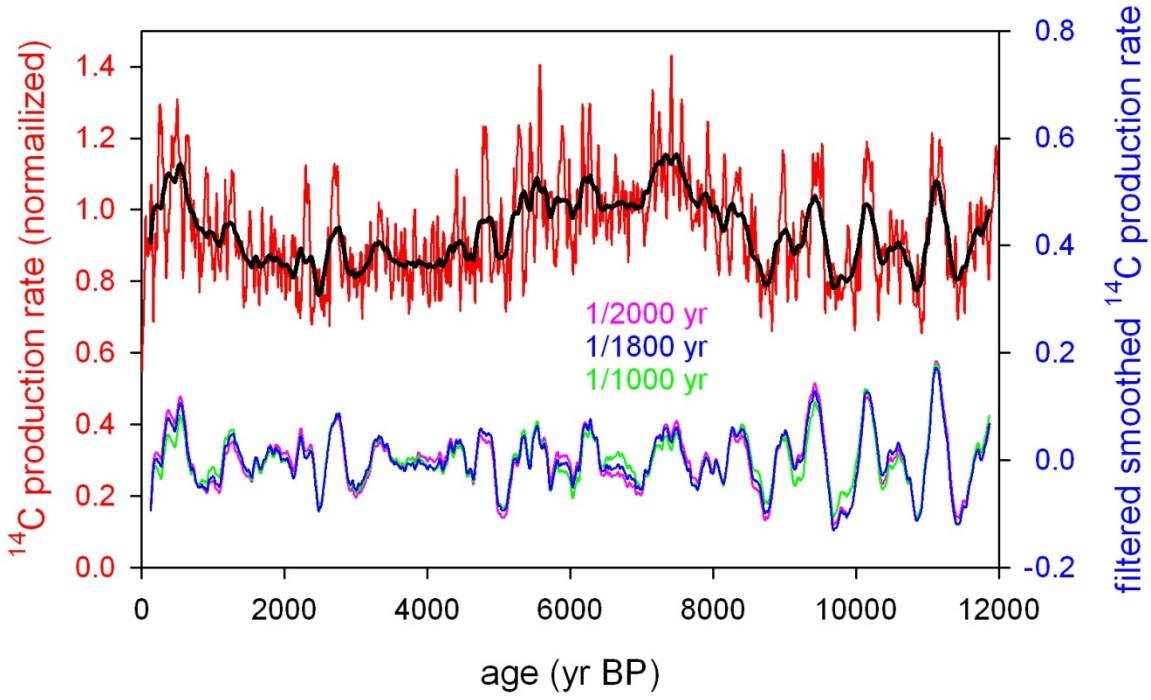

Fig. S3. Comparison of three choices for the highpass filtering of the smoothed ^{14}C production record. Shown are the normalized raw production data (red) and 251-yr running mean (black); and highpass filtered versions of the 251-yr running mean using cutoffs of 1/2000 yr (pink), 1/1800 yr (*19, 20*) (blue), and 1/1000 yr (green).

Table S1. Radiocarbon ages and calibrated ages (Calib 6.0html) for Soledad Basin core MV99-GC41/PC14.

Core	Depth	Taxa[a]	^{14}C age	age error	Reference	Accession #	Cal age[b]	1s cal range[c]	2s cal range[c]
GC41	5.5	*G. bulloides*	815	110	this study	OS-58938	250	109-406	0-471
GC41	20.5	*G. bulloides*	1470	110	this study	OS-58934	826	670-947	553-1124
GC41	50.5	*G. bulloides*	1930	170	this study	OS-58943	1286	1072-1495	881-1729
GC41	60.5	*G. bulloides*	2230	95	this study	OS-58936	1603	1434-1759	1297-1904
GC41	64	mixed planktonics	1550	35	(*1*)		894	770-1000	679-1122
GC41	85.5	*G. bulloides*	1880	130	this study	OS-58941	1229	1048-1392	896-1587
GC41	115.5	*G. bulloides*	2400	120	this study	OS-58940	1798	1603-1980	1406-2168
GC41	142	mixed planktonics	2630	45	(*1*)		2075	1930-2210	1818-2326
GC41	142	mixed benthics	2730	35	(*1*)		1955	1825-2087	1700-2245
GC41	155.5	*G. bulloides*	2780	90	this study	OS-59232	2256	2068-2428	1937-2653
GC41	181.5	*G. bulloides*	2760	75	this study	OS-59235	2228	2042-2363	1917-2599
PC14	103	mixed planktonics	3350	35	(*1*)		2955	2799-3074	2726-3226
PC14	103	mixed benthics	3610	95	(*1*)		3031	2853-3199	2730-3352
PC14	326	mixed planktonics	5150	65	(*1*)		5272	5114-5444	4951-5565
PC14	401	mixed planktonics	5810	70	(*1*)		6013	5892-6164	5731-6269
PC14	526	mixed planktonics	6580	70	(*1*)		6860	6699-7003	6568-7157
PC14	678	mixed planktonics	8070	130	(*1*)		8337	8161-8512	7967-8721
PC14	790	mixed planktonics	8820	75	(*1*)		9265	9126-9420	8982-9515
PC14	966	mixed planktonics	10100	50	(*1*)		10840	10672-11020	10569-11122
PC14	1101	mixed planktonics	10500	55	(*1*)		11356	11167-11602	11103-11755
PC14	1101	mixed benthics	10350	85	(*1*)		10888	10729-11092	10577-11172
PC14	1246	mixed planktonics	11650	80	(*1*)		12929	12787-13089	12650-13182
PC14	1396	mixed planktonics	12600	65	(*1*)		13853	13732-13994	13572-14141

[a] Depths are given in cm below top of GC or PC.
[b] $\Delta R = 200 \pm 100$ yr for planktonics and 400 ± 100 yr for benthics.
[c] Cal age ranges with <2% probability are not listed

References

1. R. W. Reynolds, N. A. Rayner, T. M. Smith, D. C. Stokes, W. Q. Wang, *Journal of Climate* **15**, 1609 (2002).
2. N. J. Mantua, S. R. Hare, Y. Zhang, J. M. Wallace, R. C. Francis, *Bulletin of the American Meteorological Society* **78**, 1069 (1997).
3. F. B. Schwing, M. O'Farrell, J. Steger, K. Baltz, *NOAA Tech. Memo.* **NOAA-TM-NMFS-SWFC-231**, 207 pp. (1996).
4. A. van Geen *et al.*, *Paleoceanography* **18**, doi:10.1029/2003PA000911 (2003).
5. M. Stuiver, P. J. Reimer, *Radiocarbon* **35**, 215 (1993).
6. P. J. Reimer *et al.*, *Radiocarbon* **51**, 1111 (2009).
7. T. M. Marchitto, S. J. Lehman, J. D. Ortiz, J. Flückiger, A. van Geen, *Science* **316**, 1456 (2007).
8. P. M. Grootes, M. Stuiver, *Journal of Geophysical Research* **102**, 26455 (1997).
9. E. A. Boyle, L. D. Keigwin, *Earth and Planetary Science Letters* **76**, 135 (1985).
10. E. A. Boyle, Y. Rosenthal, in *The South Atlantic: Present and Past Circulation,* G. Wefer, e. al., Eds. (Springer-Verlag, Berlin, 1996), pp. 423-443.
11. Y. Rosenthal, M. P. Field, R. M. Sherrell, *Analytical Chemistry* **71**, 3248 (1999).
12. T. M. Marchitto, *Geochemistry, Geophysics, Geosystems* **7**, Q05P13 (2006).
13. T. A. Mashiotta, D. W. Lea, H. J. Spero, *Earth and Planetary Science Letters* **170**, 417 (1999).
14. D. K. Pak, D. W. Lea, J. P. Kennett, *Geochem. Geophys. Geosyst.* **5**, (2004).
15. A. Grinsted, J. C. Moore, S. Jevrejeva, *Nonlinear Processes in Geophysics* **11**, 561 (2004).
16. P. J. Reimer, et al., *Radiocarbon* **46**, 1029 (2004).
17. B. M. Vinther *et al.*, *Journal of Geophysical Research-Atmospheres* **111**, (2006).
18. G. Wagner *et al.*, *Nuclear Instruments and Methods in Physics Research Section B: Beam Interactions with Materials and Atoms* **172**, 597 (2000).
19. G. Bond *et al.*, *Science* **294**, 2130 (2001).
20. R. Muscheler, J. Beer, B. Kromer, in *International Solar Cycle Studies Symposium (ISCS 2003)*. (Tatranska Lomnic, Slovakia, 2003), vol. 535, pp. 305-316.
21. U. Siegenthaler, *J. Geophys. Res.* **88**, 3599 (1983).
22. M. Stuiver, P. D. Quay, *Science* **207**, 11 (1980).
23. R. Muscheler, R. Beer, P. W. Kubik, H. A. Synal, *Quaternary Science Reviews* **24**, 1849 (2005).
24. R. C. Finkel, K. Nishiizumi, *J. Geophys. Res.-Oceans* **102**, 26699 (1997).
25. M. Vonmoos, J. Beer, R. Muscheler, *Journal of Geophysical Research-Space Physics* **111**, (2006).
26. S. J. Johnsen *et al.*, *J. Quat. Sci.* **16**, 299 (2001).
27. Y. J. Wang *et al.*, *Science* **308**, 854 (2005).
28. U. Neff *et al.*, *Nature* **411**, 290 (2001).
29. J. D. Ortiz *et al.*, *Geology* **32**, 521 (2004).